NACA TN 2063

NATIONAL ADVISORY COMMITTEE FOR AERONAUTICS

TECHNICAL NOTE 2063

A COMPARISON OF THEORETICAL AND EXPERIMENTAL WING BENDING MOMENTS DURING SEAPLANE LANDINGS

By Kenneth F. Merten, José L. Rodríguez, and Edgar B. Beck

Langley Aeronautical Laboratory
Langley Air Force Base, Va.

NACA

Washington
April 1950

NATIONAL ADVISORY COMMITTEE FOR AERONAUTICS

TECHNICAL NOTE 2063

A COMPARISON OF THEORETICAL AND EXPERIMENTAL WING BENDING MOMENTS DURING SEAPLANE LANDINGS

By Kenneth F. Merten, José L. Rodríguez, and Edgar B. Beck

SUMMARY

A smooth-water-landing investigation was conducted with a small seaplane to obtain experimental wing-bending-moment time histories together with time histories of the various parameters necessary for the prediction of wing bending moments during hydrodynamic impact. The experimental results were compared with calculated results which include inertia-load effects and the effects of air-load variation during impact. The responses of the fundamental mode were calculated with the use of the measured hydrodynamic forcing functions. From these responses, the wing bending moments due to the hydrodynamic load were calculated according to the procedure given in R. & M. No. 2221. This comparison of the time histories of the experimental and calculated wing bending moments showed good agreement both in phase relationship of the oscillations and in numerical values.

The effects of structural flexibility on the wing bending moment were large, the dynamic component of the total moment being as much as 97 percent of the static component. Changes in the wing bending moment due to the variation in air load during impact were of about the same magnitude as the static water-load component.

INTRODUCTION

Recent trends in the design of aircraft have led to an important increase of the stresses produced in wings by landing impacts. Two significant factors contributing to these increased stresses during landing are an increased proportion of the seaplane weight in the wings and an increased structural flexibility, since, in most cases, these factors have caused the ratios of the times to peak of the applied landing loads to the quarter period of the fundamental mode to approach a critical value.

Several simplified methods have been developed for determining the inertia loads in wing structures during landing impacts, and studies have been made of the landing-impact inertia loads in simplified structures with the use of the principles of these methods. (See reference 1 and bibliography.) Although experimental investigations have been made to determine the magnitudes of inertia loads in actual airplane structures (bibliography), little correlation of theory and experiment has been made concerning the nature and magnitude of inertia loads in airplane wings during actual landing impacts.

Another aspect of the problem of wing loads during landing is the variation of air load due to changes of attitude and flight path during impact. The importance of this change in air load has been the subject of some speculation but little investigation.

In order to evaluate the importance of the various components of the load, including dynamic effects and variation in air load, data were obtained during full-scale landing tests of a small seaplane to provide a comparison of actual wing loads with those predicted by a simplified method (reference 1).

The present paper gives a comparison of the theoretical and experimental wing loads, in the form of time histories of the wing bending moments, and discusses the contributions of each of the components of the moment (static water-load moment, dynamic water-load moment, and air-load moment) to the total. The static and dynamic components of the total moment were calculated and combined according to the procedure of reference 1, with the responses of the fundamental mode being calculated from the recorded time histories of the applied forces. The air-load component was calculated by the procedure of the appendix.

SYMBOLS

C_L lift coefficient $\left(\frac{2L}{\rho S V^2}\right)$

g acceleration due to gravity (32.2 ft/sec^2)

L lift, pounds

M bending moment in wing, pound-inches

n load factor, multiples of g

S wing surface area, square feet

T	duration of impact, seconds
t	time, seconds
t_i	time to peak of applied load, seconds
t_n	natural period of fundamental mode, seconds
u	dynamic response factor, ratio of maximum total water-load wing bending moment to maximum static water-load bending moment
V	velocity of seaplane, feet per second
α	angle of attack, degrees
γ	flight-path angle, degrees
Δ	prefix denoting change
ρ	density, slugs per cubic foot
σ	response
σ_s	static response
τ	trim angle, degrees
ω	circular frequency, cycles per second

Subscripts:

av	average
c	corrected for air load
h	horizontal
n	normal to keel
o	at time of water contact
p	parallel to keel
r	recorded

T	total
v	vertical
max	maximum

APPARATUS AND INSTRUMENTATION

The airplane used in the present investigation was a small two-engine seaplane (fig. 1). Pertinent information about the seaplane is given in table I, and additional information may be obtained from reference 2. The frequency and shape of the fundamental wing bending mode were found from ground vibration tests and are given in table II and figure 2. The spanwise weight distribution is also given in table II.

The trim variation was measured with a gyroscopic trim recorder mounted in the cabin floor. The airspeed was measured with an NACA airspeed recorder, pitot-static-tube type, mounted above the cabin. Accelerations of the center of gravity were obtained from an NACA optical-recording three-component accelerometer mounted securely in the fuselage near the center of gravity. The time of contact was determined from a water-contact indicator located on the keel at the main step. The hull immersions were determined from pressure gages installed along the bottom of the hull. The wing bending moments were measured by means of a strain gage mounted on the wing main spar 9 inches from the center line of the seaplane (hereinafter referred to as station 9).

The estimated accuracies of the experimental data based on calibration, instrument, and reading error are as follows:

Horizontal velocity, V_h, feet per second	±4
Trim angle, τ, degrees	±0.25
Load factor, n, multiples of g	±0.2
Initial wing lift, L_o, multiples of g	±0.05
Total wing bending moment, M_T, pound-inches	$\pm 0.05 \times 10^6$

TEST PROCEDURE

The landing-impact tests were made in smooth water. During these landing tests, airspeed, trim variation, center-of-gravity accelerations, and wing-spar bending moments were recorded. The landings were made at horizontal velocities ranging from 95.4 to 112.0 feet per second, trim

angles ranging from 3.00° to 7.83°, and initial flight-path angles ranging from 2.0° to 4.4°. The resulting maximum center-of-gravity accelerations normal to the keel line ranged from 1.10g to 1.96g and the duration of the impacts varied from 0.63 to 0.87 second. The times to peak of these normal accelerations ranged from 0.10 to 0.36 second. Values of these parameters and other pertinent information for all the tests are presented in table III.

THEORY

Williams' Method

In reference 1 a method was proposed for calculating the dynamic effect of an impulsive load applied to an elastic structure. Basically, the method follows classical normal-mode vibration theory by considering the total response of the elastic structure to a forcing function at any instant to be the summation of the responses of all of its normal modes at that instant. However, a unique feature of the method is that the total response of each mode is separated into a static and a dynamic component, and the stress due to the sum of the static components of the responses of all the modes is found in one calculation by rigid-body analysis. This stress is referred to as the static-load stress. The stress of each mode due to its dynamic component of response is found separately. The total stress is the sum of the static-load stress and the dynamic components of stress for the significant modes. Time histories of stress are found in these calculations and thus phase relationships of the modes are considered when the stresses for each mode are added.

Air-Load Variation

Equations are developed in the appendix for determining the effect of air-load variation on the wing bending moment during impact. The change in bending moment at any instant is expressed in terms of the ratio of bending moment to lift at time of contact and the wing lift at that instant. In developing the equations, the air load is assumed to change instantaneously with change in angle of attack and the rate of change in air load is assumed to be slow enough to neglect structural dynamic response. Also, the ratio of bending moment to lift is assumed to be constant throughout the impact.

CALCULATIONS AND RESULTS

The variations of the wing angle of attack and velocity during impact necessary for computing the changes in bending moment by equation (4) of the appendix were determined for each impact from the recorded data in the following manner. The accelerations normal and parallel to the keel line, obtained from the three-component center-of-gravity accelerometer, were plotted (fig. 3). After the trim-angle variation (fig. 4(a)) was taken into account, these accelerations were resolved into vertical and horizontal components. Integration of the time histories of these accelerations over the duration of the impact produced time histories of the changes in vertical and horizontal velocities. Since the vertical velocity at the time of contact was not accurately known, the initial velocity was determined so that integration of the time-history curve over the duration of the impact resulted in a final vertical displacement of zero. (The duration of the impact is defined as the interval between the time of contact and the time when the center of gravity again reached its initial height above the mean water line. The instant of contact was found from a water-contact indicator on the step and the time history of the center-of-gravity displacement was determined from the times of immersion and emersion of the hull pressure gages, the fixed location of the center of gravity relative to the step, and trim-angle time history.) Integration of the time-history curve of the corrected vertical velocity from time of contact to the time of zero vertical velocity determined the maximum displacement of the center of gravity. The maximum displacements determined in this manner for all the impacts agreed within experimental error with the maximum displacements calculated from the hull pressure gages. With the use of the corrected vertical-velocity and horizontal-velocity time histories, time histories of the flight-path angle γ and the resultant velocity were computed. From the time histories of trim angle τ (fig. 4(a)) and flight-path angle γ (fig. 4(b)), the time history of the angle of attack α was computed (fig. 4(c)).

With the use of the time histories of angle of attack and resultant velocity, the changes in bending moment in the wing at station 9 due to the changes in air load were determined for each impact by use of the equations in the appendix and are presented in parts (a) of figures 5 to 10.

The procedure of reference 1 was used to compute the bending moments because it provides a convenient means of applying the principles essential to a dynamic-loads analysis which results in time histories of the wing bending moments. The forcing function for each impact was determined from the normal acceleration measured in the hull by an accelerometer located near the seaplane center of gravity. Because of

the manner of connection between the wing and hull (fig. 1), the measured acceleration was not appreciably affected by the oscillations of the wing. By including the effect of the varying wing lift on the center-of-gravity acceleration, the acceleration normal to the keel line due to the hydrodynamic force only was determined. From this acceleration and the mass of the seaplane, the hydrodynamic forcing function was calculated. The dynamic responses of the significant modes to this forcing function were computed by a recurrence method developed at the Langley Structures Research Division in which the actual forcing function is used without approximation. Only the dynamic effects of the fundamental bending mode were included in the final results because calculations showed the dynamic effects of the second symmetrical bending mode to be negligible. This observation was borne out by the absence of higher mode effects on the strain-gage records. The calculated time histories of the static water-load and dynamic water-load components of wing bending moment at station 9 are presented in parts (a) of figures 5 to 10. The spanwise bending-moment distribution for the fundamental-mode 1 g inertia loading calculated as set forth in reference 1, a 1 g static water loading, and a level-flight loading are plotted in figure 11. The values of the bending moment at station 9 used in the application of the method of reference 1 were obtained from this plot.

These three components of wing-bending-moment changes obtained in this manner for station 9 were combined and added to the wing bending moment existing at the instant of contact. This total theoretical wing bending moment is presented in parts (b) of figures 5 to 10 together with the wing-bending-moment variation measured by the strain gage at station 9.

In order to demonstrate the accuracy gained by using the actual forcing function, responses were computed for two typical impacts with the use of apparently good approximations to the recorded forcing functions. Parts (a) of figures 12 and 13 show the actual forcing functions for these impacts together with the approximations. The responses to the approximations are presented in parts (b) of figures 12 and 13 together with the responses obtained from the actual forcing functions with the use of the recurrence method.

DISCUSSION

Comparisons between the total theoretical and experimental wing bending moments are presented in parts (b) of figures 5 to 10. The comparisons are made only for wing station 9 because the bending moments in the outer wing section were so small as to be of the same order as the estimated error. Only the dynamic effects of the fundamental

bending mode were included in the final results because calculations showed the dynamic effects of the second symmetrical bending mode to be negligible. This negligibility was borne out by the absence of higher-mode effects on the strain-gage records. The comparisons show the predicted values to be in good agreement with the experimental values. As can be seen from the figures, the phase relationships between the theoretical and experimental values are consistently good, and the maximum changes from initial conditions show a range of error of 5 to 28 percent based on the experimental values of the maximum changes in wing moment. These results indicate that when the three components of moment are included in the theory, good agreement is obtained.

A comparison of the level-flight bending moment and the change in bending moment due to the heaviest impact of the tests shows that the maximum change in bending moment accompanying a downward motion of the wing was approximately 50 percent of the level-flight moment (figs. 11 and 5(b)). This maximum bending-moment change was produced by a 2.03g impact. When any differences in the response factor and any change in air-load bending moment are neglected, landings of over 4g would be required for the downward motion of the wing merely to start stress reversal in the wing. Similarly, even if the maximum dynamic water-load bending moment (fig. 8(a)) caused by a 1.94g impact were to be twice as large for a 4g impact, were to exist after the water load was removed, and were to be superposed on a level-flight moment, the moment produced by the upward motion of the wing would still be less than twice the level-flight moment. Therefore, the change in bending moment due to a landing impact is unimportant in this seaplane insofar as this change will not produce critical stresses at the wing root. This unimportance may be largely attributed to the fact that the fundamental-mode 1 g inertia loading is relatively small as compared with a level-flight loading (fig. 11).

The effects of structural flexibility on the computed bending moments can be seen by comparing the static and dynamic components of the water-load bending moment in parts (a) of figures 5 to 10 and by observing the dynamic response factors u in table III. The dynamic overstress attributable to structural flexibility is the dynamic component of stress in parts (a) of figures 5 to 10 and is represented in the response factor u by the amount that this factor differs from unity. Since response factors as high as 1.97 are obtained, the dynamic overstress sometimes contributes an increment of stress almost as large as the static water-load stress. This observation is in agreement with the results of other investigators (bibliography) and shows the necessity of using dynamic analyses in landing-load investigations.

The change in wing bending moment due to change in air load on the wing is a function of the changes in velocity and angle of attack. (See

the appendix.) In these tests the changes in velocity during the impacts were small (table III) and the changes in air-load bending moment were therefore almost entirely attributable to the changes in angle of attack. Since the angle of attack is a function of the trim and flight-path angles, large changes in angle of attack will occur when the trim and flight-path angles change to a great degree. For the relatively small changes in trim angle and flight-path angle which occurred in these tests (the maximum values being 9.31° and 7.0°, respectively), air-load changes as large as 0.2g were computed. For this airplane, these changes in air-load bending moment were of about the same magnitude as the bending-moment changes due to the static component of loading (parts (a) of figs. 5 to 10) and inclusion of the effects of air-load changes in the calculations was therefore necessary. For other airplanes with structural and mass characteristics conducive to larger inertia-load moments, the bending-moment changes accompanying a 0.2g change in air load would be small relative to the changes in bending moment caused by inertia loads. However, for more severe changes in flight-path angle, which should be considered in a design analysis, the effects of the change in air load on the bending moment in the wing may still be large enough to warrant consideration in a design analysis. Further investigation is necessary to determine the importance of this air-load variation in design-strength calculations.

In most landing tests the applied forcing functions are not easily obtained from the center-of-gravity accelerations because of the superposed accelerations caused by structural oscillations. But because the fuselage of this airplane is connected to the wing by struts located near the nodal point of the fundamental mode which represented the greatest portion of the wing bending and by a nonstructural fairing which neither transmitted nor interfered with the wing oscillations, the accelerometer in the fuselage was not appreciably affected by the wing oscillations in these tests.

The calculation of the dynamic response of each of the normal modes of the seaplane involves solving for the response of an equivalent simple mass oscillator to the given forcing function. In this calculation it is common practice to approximate the forcing function in order to simplify the computation. In order to indicate the effect of such approximations on the accuracy of the response, figures 12 and 13 have been prepared. In these figures are shown two typical forcing functions, various simple approximations to each, and the responses computed from the two forcing functions and their approximations. By comparing the calculated responses of the approximations to those of the recorded forcing functions in figures 12(b) and 13(b), it is seen that errors as large as 20 percent in the total response may be introduced into the calculations by use of apparently good approximations. A recurrence method developed by the Langley Structures Research Division was used to compute the total responses to the recorded

forcing functions used in preparing figures 12 and 13. In this procedure the motion of each of the significant normal modes of the airplane is computed from the equation of motion of an equivalent simple mass oscillator subjected to the recorded forcing function. Figures 14(a) and 14(b) have been prepared to show the accuracy with which the total response of the equivalent simple mass oscillator can be obtained by this procedure. Comparison is made of the ratios of the total response σ to the maximum static response of the normal mode $\sigma_{s_{max}}$ for simple sinusoidal and triangular forcing functions calculated by both this method and Duhamel's integral. It can be seen that excellent agreement is obtained.

CONCLUSIONS

Experimental wing bending moments obtained from a landing-impact investigation with a small full-scale seaplane were compared with analytical results. The effects of the variation in air load during the impacts were included in the analytical procedure. The responses of the fundamental mode were calculated from the recorded time histories of the applied hydrodynamic forces. For the seaplane tested and the conditions of the impacts encountered, the following conclusions may be drawn:

1. Good agreement between measured and computed wing bending moments was obtained when the three components of the wing moment (static water-load moment, dynamic water-load moment, and air-load moment) were included in the calculations.

2. The effects of structural flexibility on the wing bending moments, represented by the dynamic overstress and understress, were large, the moment due to the dynamic component of the total response being as much as 97 percent of that caused by the static water-load component.

3. Although the changes in seaplane attitude during the landing impacts were small, the variation in the air-load component of the total moment was of about the same magnitude as the static water-load component. Although this comparison of changes is not representative of the relative importance of the air-load variation in seaplanes with structures conducive to large inertia-load components, it indicates the probable significance of the effects of air-load variation since large changes in seaplane attitude must also be considered.

Langley Aeronautical Laboratory
National Advisory Committee for Aeronautics
Langley Air Force Base, Va., December 21, 1949

APPENDIX

DETERMINATION OF THE EFFECT OF CHANGE IN AIR LOAD ON WING BENDING MOMENT

In order to determine the effect of change in air load on the bending moment in the wing during impact, a procedure was developed to determine the moment at any time t in terms of the ratio of bending moment to lift at time of contact and the wing lift at time t. The ratio of bending moment to lift was assumed to be constant, or

$$\frac{M}{L} = \frac{M_o}{L_o}$$

Therefore,

$$M = \frac{M_o}{L_o} L$$

or

$$M = \frac{M_o}{L_o} \frac{1}{2} \rho S V^2 C_L$$

The ratio M_o/L_o was obtained from initial conditions. The change in moment may be expressed as

$$M_o - M = \frac{M_o}{L_o} \frac{1}{2} \rho S V_o{}^2 C_{L_o} - \frac{M}{L} \frac{1}{2} \rho S V^2 C_L$$

or

$$\Delta M = \frac{M_o}{L_o}\frac{1}{2}\rho S V_o^2 C_{L_o}\left(1 - \frac{V^2 C_L}{V_o^2 C_{L_o}}\right) \qquad (1)$$

The numerical value of C_{L_o} may be calculated from the lift equation and initial conditions. Therefore,

$$nW = \frac{1}{2}\rho S V_o^2 C_{L_o}$$

or

$$C_{L_o} = \frac{nW}{\frac{1}{2}\rho S V_o^2}$$

where n is the acceleration in multiples of g acting on the seaplane at contact and W is the seaplane weight in pounds.

From the curve of C_L plotted against α (no flaps) supplied by the manufacturer, the initial conditions were found to lie in the straight portion of the curve for all impacts considered. The equation for C_L may therefore be expressed as

$$C_L = K + m\alpha \qquad (2)$$

where K is the C_L intercept at $\alpha = 0^\circ$ and m is the slope of the curve. The value of K was determined from the initial conditions of the impacts. Since the slope of the curve of C_L plotted against α is constant regardless of flap setting, an average value of K was believed to be usable, provided the error in calculating the lift with the use of this average value would not be greater than that estimated

for the recording instruments. Accordingly, such a procedure was carried out and the maximum error was 3.6 percent. Since the slope of the lift curve is known to be 0.0498, equation (2) may be written

$$C_L = K_{av} + 0.0498\alpha \tag{3}$$

Substitution of equation (3) in equation (1) for C_L results in

$$\Delta M = \frac{M_o}{L_o}\frac{1}{2}\rho S V_o^2 C_{L_o}\left[1 - \frac{V^2(K_{av} + 0.0498\alpha)}{V_o^2 C_{L_o}}\right]$$

or

$$\Delta M = B\left[1 - \frac{V^2(K_{av} + 0.0498\alpha)}{C}\right] \tag{4}$$

where

$$B = \frac{M_o}{L_o}\frac{1}{2}\rho S V_o^2 C_{L_o}$$

$$C = V_o^2 C_{L_o}$$

Equation (4) expresses the change in bending moment ΔM due to change in air load in terms of initial conditions and measured variables.

REFERENCES

1. Williams, D., and Jones, R. P. N.: Dynamic Loads in Aeroplanes under Given Impulsive Loads with Particular Reference to Landing and Gust Loads on a Large Flying Boat. R. & M. No. 2221, British A.R.C., Sept. 1945.

2. Steiner, Margaret F.: Comparison of Over-All Impact Loads Obtained during Seaplane Landing Tests with Loads Predicted by Hydrodynamic Theory. NACA TN 1781, 1949.

BIBLIOGRAPHY

Simplified Methods

Biot, M. A., and Bisplinghoff, R. L.: Dynamic Loads on Airplane Structures during Landing. NACA ARR 4H10, 1944.

Goland, M., Luke, Y. L., and Kahn, Elizabeth A.: Prediction of Dynamic Landing Loads. Tech. Rep. No. 5815, ATI No. 53340, Air Materiel Command, U. S. Air Force, Jan. 30, 1949.

Jenkins, E. S., and Pancu, C. D. P.: Dynamic Loads on Airplane Structures. Preprint for presentation at the SAE National Aeronautic and Air Transport Meeting. April 13-15, 1948.

Mayo, Wilbur L.: Solutions for Hydrodynamic Impact Force and Response of a Two-Mass System with an Application to an Elastic Airframe. NACA TN 1398, 1947.

Pryor, H. E.: Theoretical and Experimental Dynamic Landing Accelerations on a Model Wing. Document No. D-9423, Boeing Aircraft Co. (Seattle), Nov. 5, 1948.

Application of Simplified Methods to Simplified Structures

Bisplinghoff, R. L., Isakson, G., Pian, T. H. H., Flomenhoft, H. I., and O'Brien, T. F.: An Investigation of Stresses in Aircraft Structures under Dynamic Loading. Contract No. NOa(s) 8790, M.I.T. Rep., Bur. Aero., Jan. 21, 1949.

Pian, T. H. H., and O'Brien, T. F.: Further Developments in Methods of Transient Stress Analysis during Landing. Contract No. NOa(s) 8790, M.I.T. Rep., Bur. Aero., July 1, 1949.

Ramberg, Walter: Transient Vibration in an Airplane Wing Obtained by Several Methods. Res. Paper RP1984, Nat. Bur. of Standards Jour. Res., vol. 42, no. 5, May 1949, pp. 437–447.

Stowell, Elbridge Z., Houbolt, John C., and Batdorf, S. B.: An Evaluation of Some Approximate Methods of Computing Landing Stresses in Aircraft. NACA TN 1584, 1948.

Stowell, Elbridge Z., Schwartz, Edward B., and Houbolt, John C.: Bending and Shear Stresses Developed by the Instantaneous Arrest of the Root of a Cantilever Beam Rotating with Constant Angular Velocity about a Transverse Axis through the Root. NACA ARR L5E25, 1945.

Stowell, Elbridge Z., Schwartz, Edward B., and Houbolt John C.: Bending and Shear Stresses Developed by the Instantaneous Arrest of the Root of a Moving Cantilever Beam. NACA Rep. 828, 1945.

Stowell, Elbridge Z., Schwartz, Edward B., Houbolt, John C., and Schmieder, Albert K.: Bending and Shear Stresses Developed by the Instantaneous Arrest of the Root of a Cantilever Beam with a Mass at Its Tip. NACA MR L4K30, 1944.

Wasserman, L. S.: A Simplified Procedure for Computing Transient Responses of Linear Systems to Landing Gear Impulses. MR No. TSEAC5-4595-5-4, Air Materiel Command, Eng. Div., U.S. Air Force, Aug. 8, 1947. (Also available from CADO, ATI 10819.)

Wasserman, L. S., and Kramer, E. H.: A Method for Predicting Dynamic Landing Loads. MR No. MCREXA5-4595-8-2, Air Materiel Command, Eng. Div., U.S. Air Force, Feb. 20, 1948.

Williams, D.: Displacements of a Linear Elastic System under a Given Transient Load. British S.M.E. C/7219/DW/19, Aug. 1946.

Experimental Studies with Actual Airplanes

Kramer, Edward H.: Dynamic Landing Loads of an AT-11 Airplane. MR No. TSEAL2-45128-2-12, Air Materiel Command, Eng. Div., U.S. Air Force, Aug. 27, 1945. (Also available from CADO, ATI 16478.)

Strickland, J. T.: Acceleration Data on B-24 Dynamic Landing Load Tests. MR No. TSEAL-2-4263-46-6, Air Technical Service Command, Eng. Div., Army Air Forces, Dec. 9, 1944. (Also available from CADO, ATI 17137.)

Westfall, John R.: Accelerations Measured at Center of Gravity and along Span of the Wing of a B-24D Airplane in Landing Impacts. NACA MR, Aug. 10, 1944.

Application of Simplified Methods to Actual Airplanes

Savitsky, Daniel: Theoretical and Experimental Wing-Tip Accelerations of a Small Flying Boat during Landing Impacts. NACA TN 1690, 1948.

TABLE I

GENERAL INFORMATION ABOUT SEAPLANE USED IN

LANDING-IMPACT INVESTIGATION

Approximate flying weight during tests, lb	19,200
Stalling speed (flaps down), fps	94
Wing area, sq ft	780.6
First natural frequency, cps	4.76
Second natural frequency, cps	13.0

TABLE II

WEIGHT DISTRIBUTION AND MODE-SHAPE FACTOR FOR FUNDAMENTAL BENDING (4.76 cps) MODE OF WING SEMISPAN

Distance from center line (in.)	Associated station weight (lb)	Mode-shape factor
0	----	-0.045
31	881	-.044
75	2057	-.026
87.7	5076	-.022
119	881	-.004
170	116	.053
210	102	.110
250	88	.190
290	181	.270
330	64	.370
370	53	.490
410	43	.625
440	18	.730
477.7	40	.860
516	----	1.000
Total	9600	

TABLE III

FLIGHT AND IMPACT VARIABLES

Run	V_{h_o} (fps)	$\Delta V_{h_{max}}$ (fps)	V_{v_o} (fps)	$\Delta V_{v_{max}}$ (fps)	$\frac{\Delta V_v}{\Delta V_h}$	$n_{n_{r_{max}}}$	$n_{n_{o_{max}}}$	$n_{p_{max}}$	$n_{v_{max}}$	$n_{n_{max}}$	$n_{v_{av}}$	$n_{h_{av}}$	$\frac{n_{h_{av}}}{n_{v_{av}}}$	T (sec)	$\frac{t_1}{t_n/4}$	ΔM_{max} (lb-in)	u	τ_o (deg)	$\Delta\tau_{max}$ (deg)	α_o (deg)	$\Delta\alpha_{max}$ (deg)	$\Delta\gamma_{max}$ (deg)
1	103.0	4.91	5.1	8.37	0.587	1.96	2.03	0.264	1.90	0.508	0.377	0.221	0.587	0.69	3.78	0.575×10^6	1.47	7.83	1.30	10.66	5.20	4.7
2	95.4	3.55	3.5	7.29	.487	1.21	1.26	.181	1.19	.259	.260	.127	.487	.87	6.28	.250	1.23	6.01	5.07	8.11	2.10	4.2
3	100.5	3.46	7.2	11.29	.307	1.61	1.69	.209	1.59	.340	.625	.191	.304	.65	3.43	.410	1.53	5.72	5.21	9.82	4.36	6.5
4	112.0	3.83	8.6	13.64	.281	1.90	1.94	.255	1.89	.355	.689	.190	.276	.63	1.90	.483	1.97	3.00	9.31	7.39	4.45	7.0
5	105.9	3.54	4.4	8.10	.437	1.16	1.24	.183	1.14	.285	.329	.143	.435	.77	4.95	.345	1.42	6.07	4.28	8.45	3.29	4.4
6	104.1	3.42	3.6	6.90	.495	1.10	1.19	.208	1.07	.310	.268	.133	.496	.80	6.85	.335	1.13	7.39	3.30	9.34	2.67	3.8

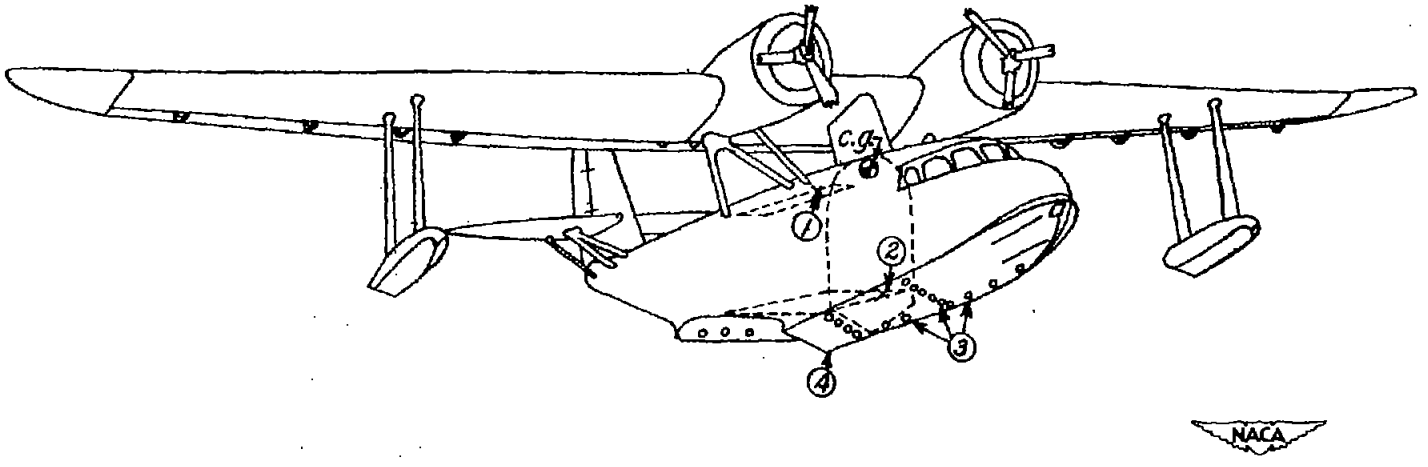

1. NACA optical-recording three-component accelerometer
2. Gyroscopic trim recorder
3. Pressure gages and water contacts
4. Water-contact indicator

Figure 1.- Seaplane and instrumentation.

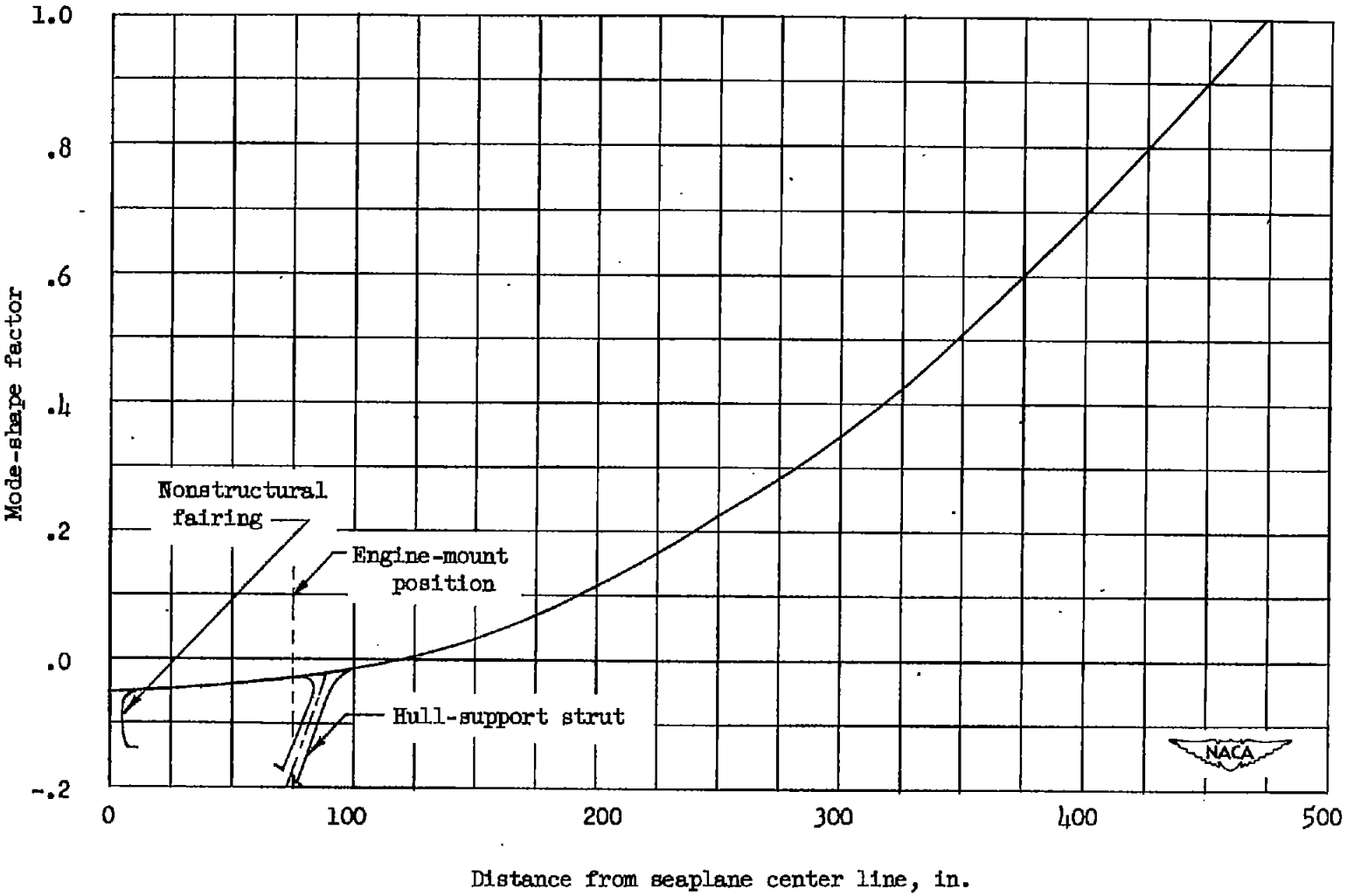

Figure 2.- Experimental fundamental bending-mode shape of wing semispan. Frequency, 4.76 cycles per second.

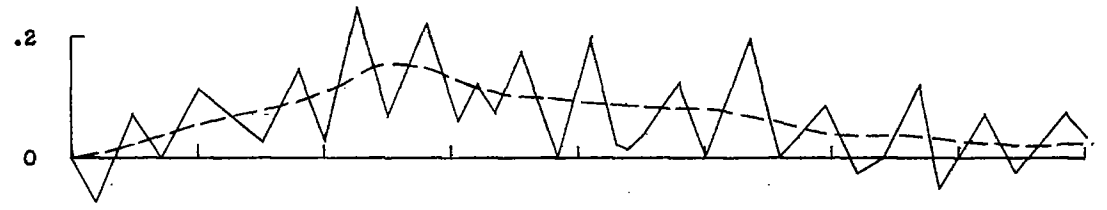

(a) Acceleration parallel to seaplane keel line during impact.

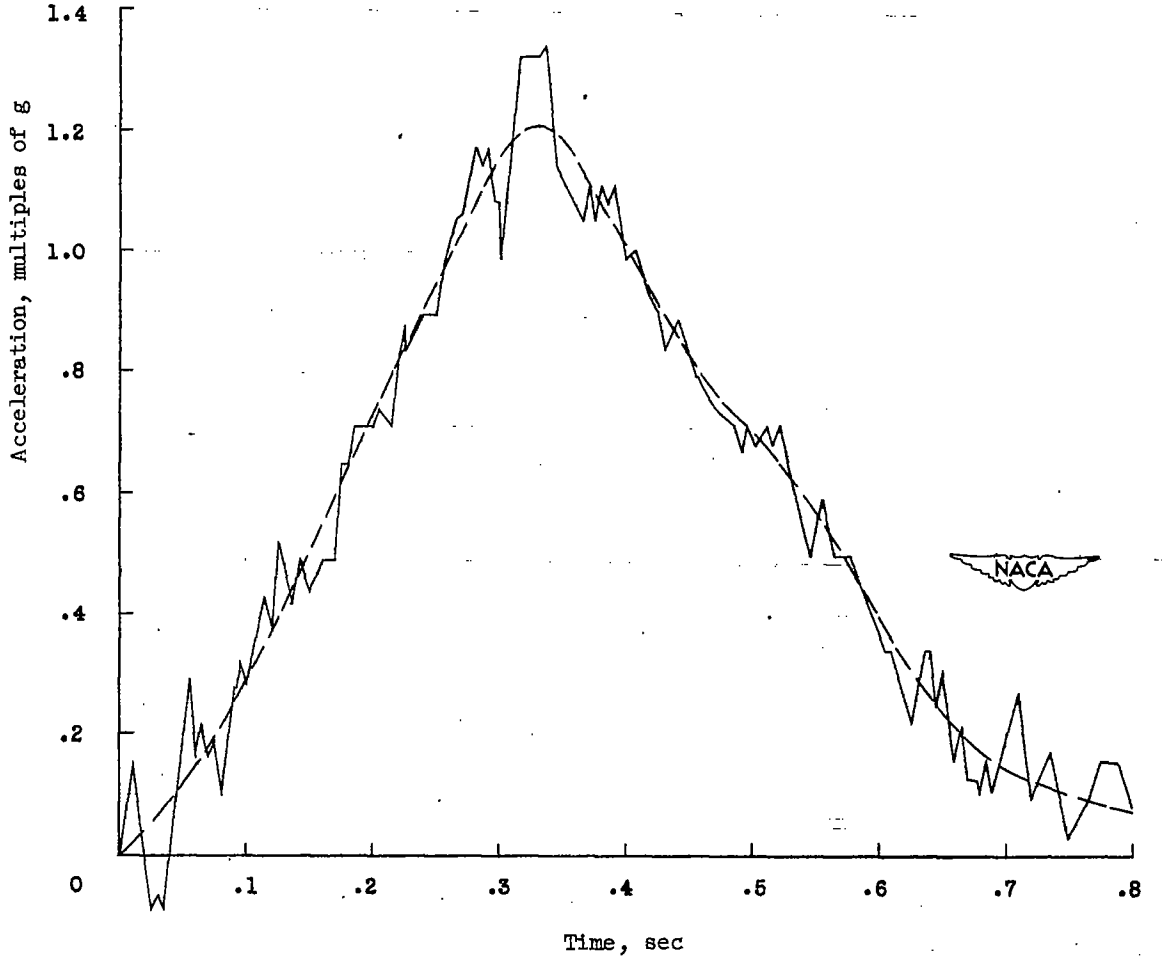

(b) Acceleration normal to seaplane keel line during impact.

Figure 3.- Typical accelerometer records and fairings.

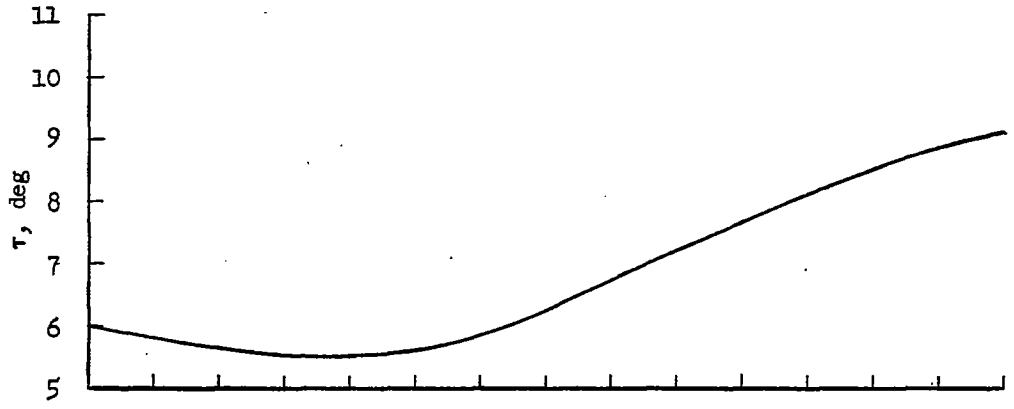

(a) Trim-angle variation during impact.

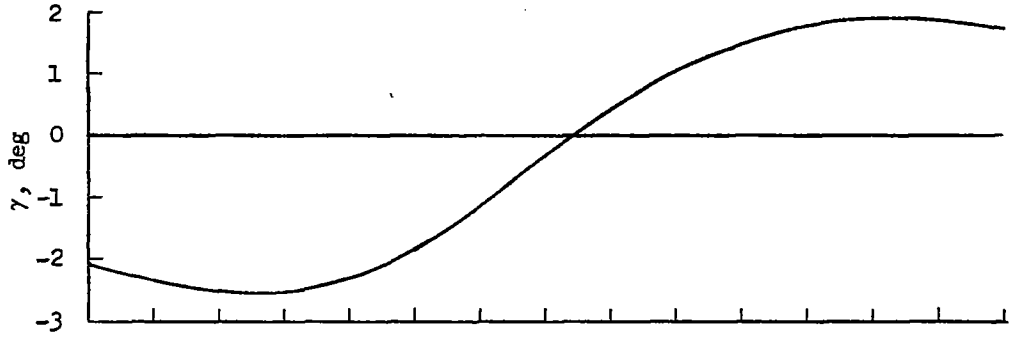

(b) Flight-path-angle variation during impact.

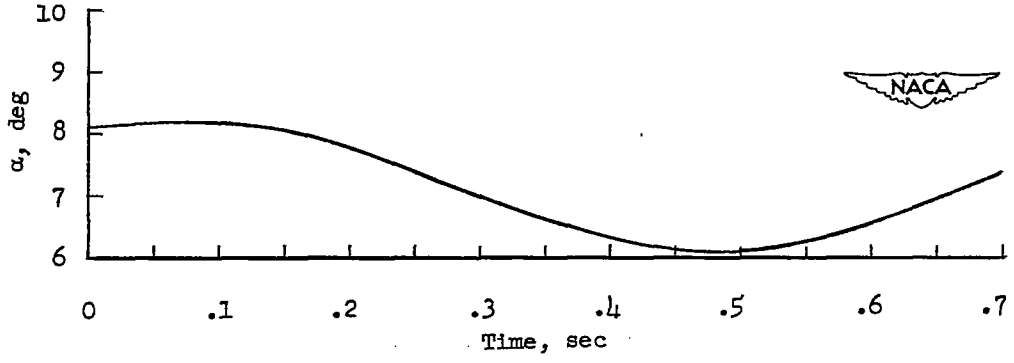

(c) Angle-of-attack variation during impact.

Figure 4.- Typical time histories of pitching motion based on recorded and calculated data.

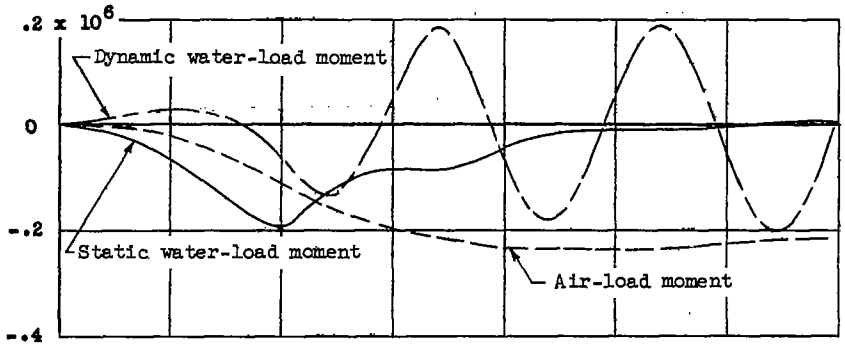

(a) Components of wing-bending-moment changes during impact.

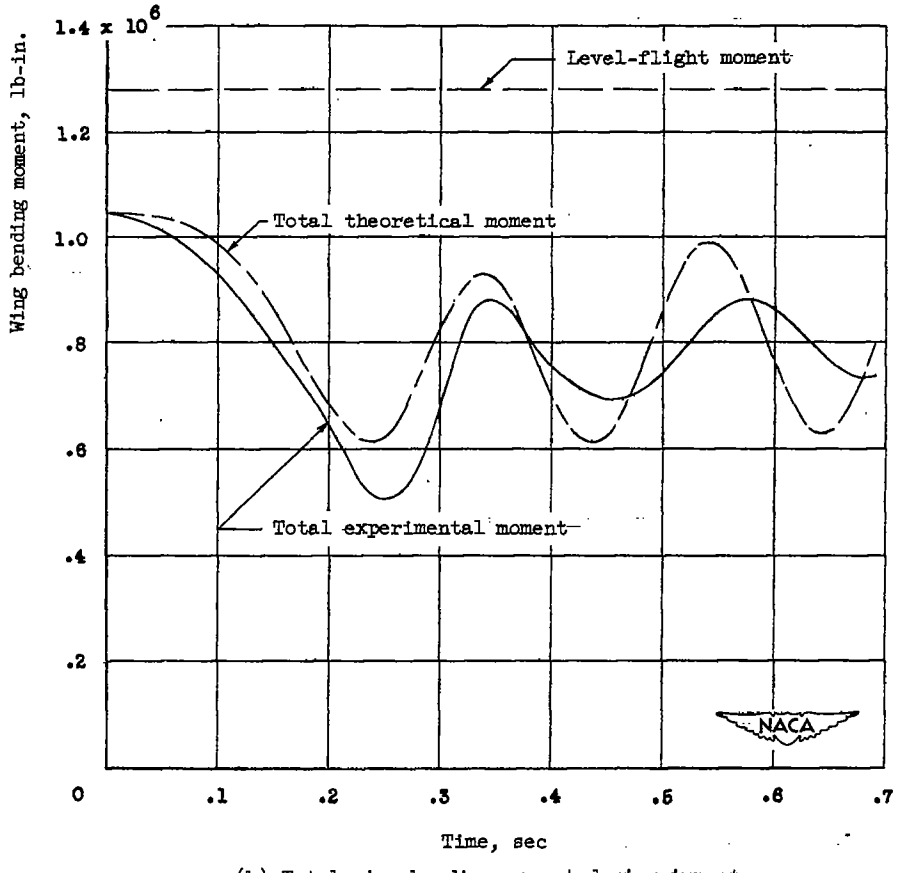

(b) Total wing bending moment during impact.

Figure 5.- Wing-bending-moment time histories during impact, run 1.

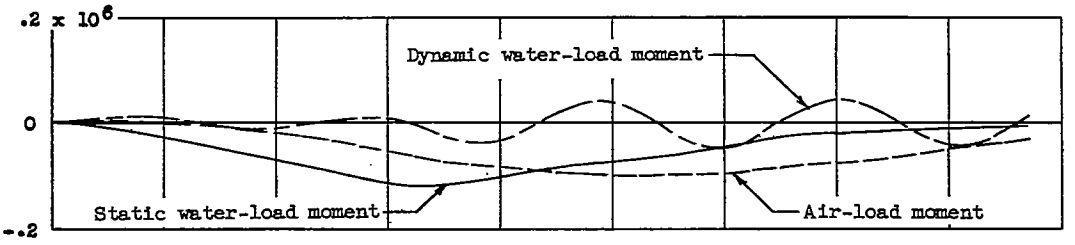

(a) Components of wing-bending-moment changes during impact.

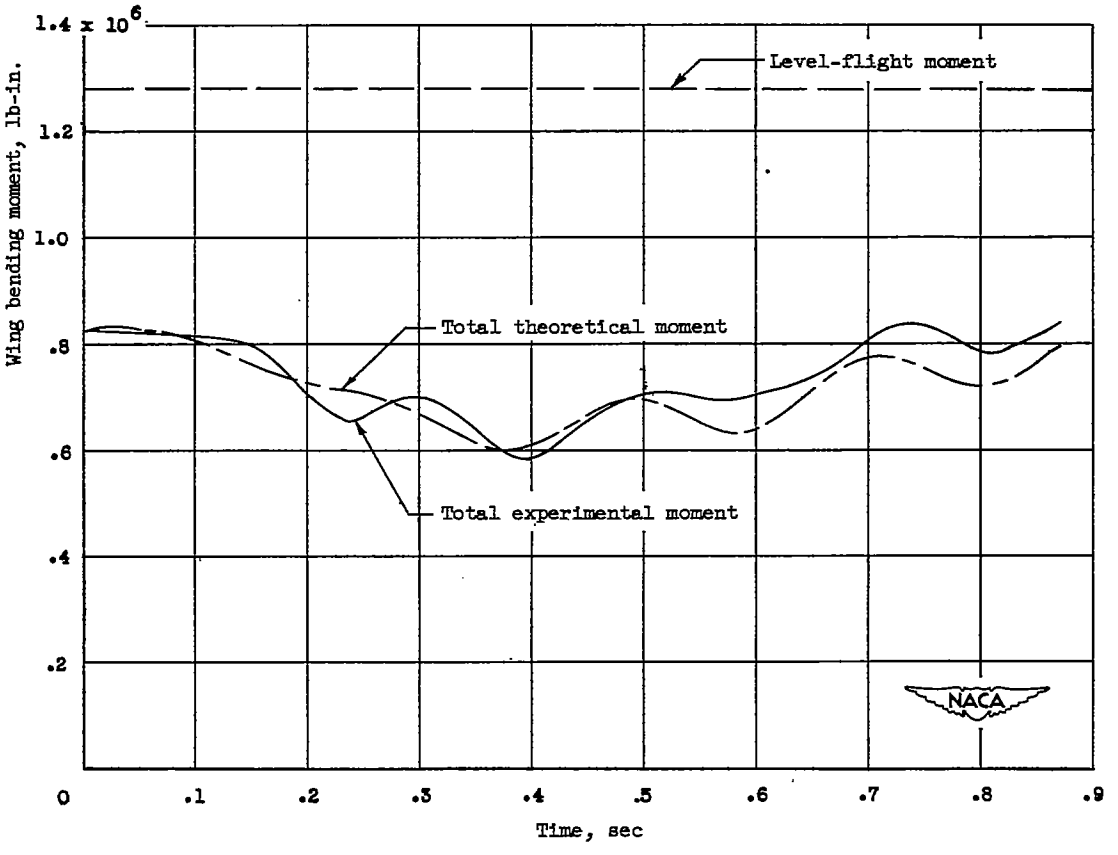

(b) Total wing bending moment during impact.

Figure 6.- Wing-bending-moment time histories during impact, run 2.

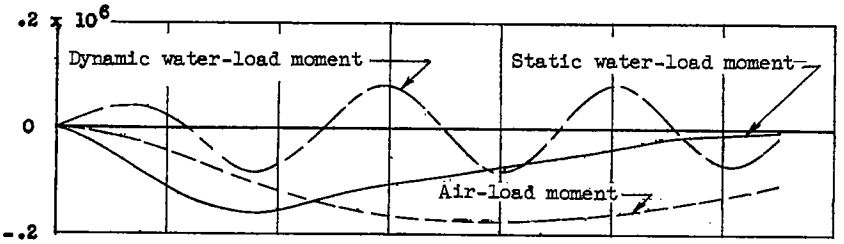

(a) Components of wing-bending-moment changes during impact.

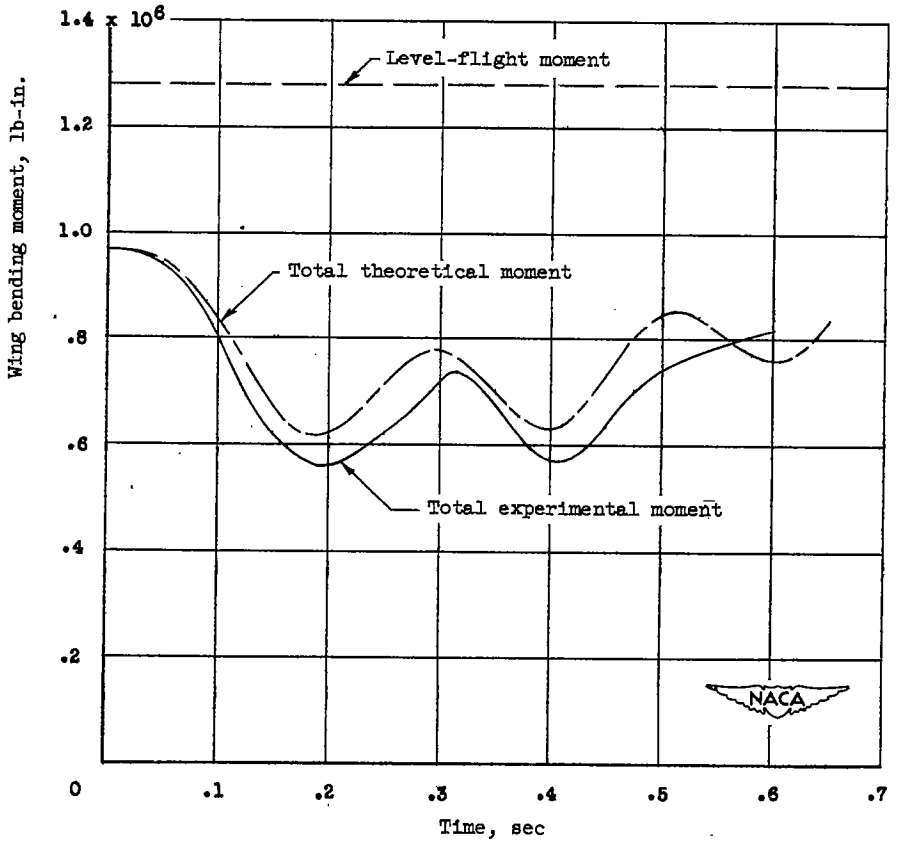

(b) Total wing bending moment during impact.

Figure 7.- Wing-bending-moment time histories during impact, run 3.

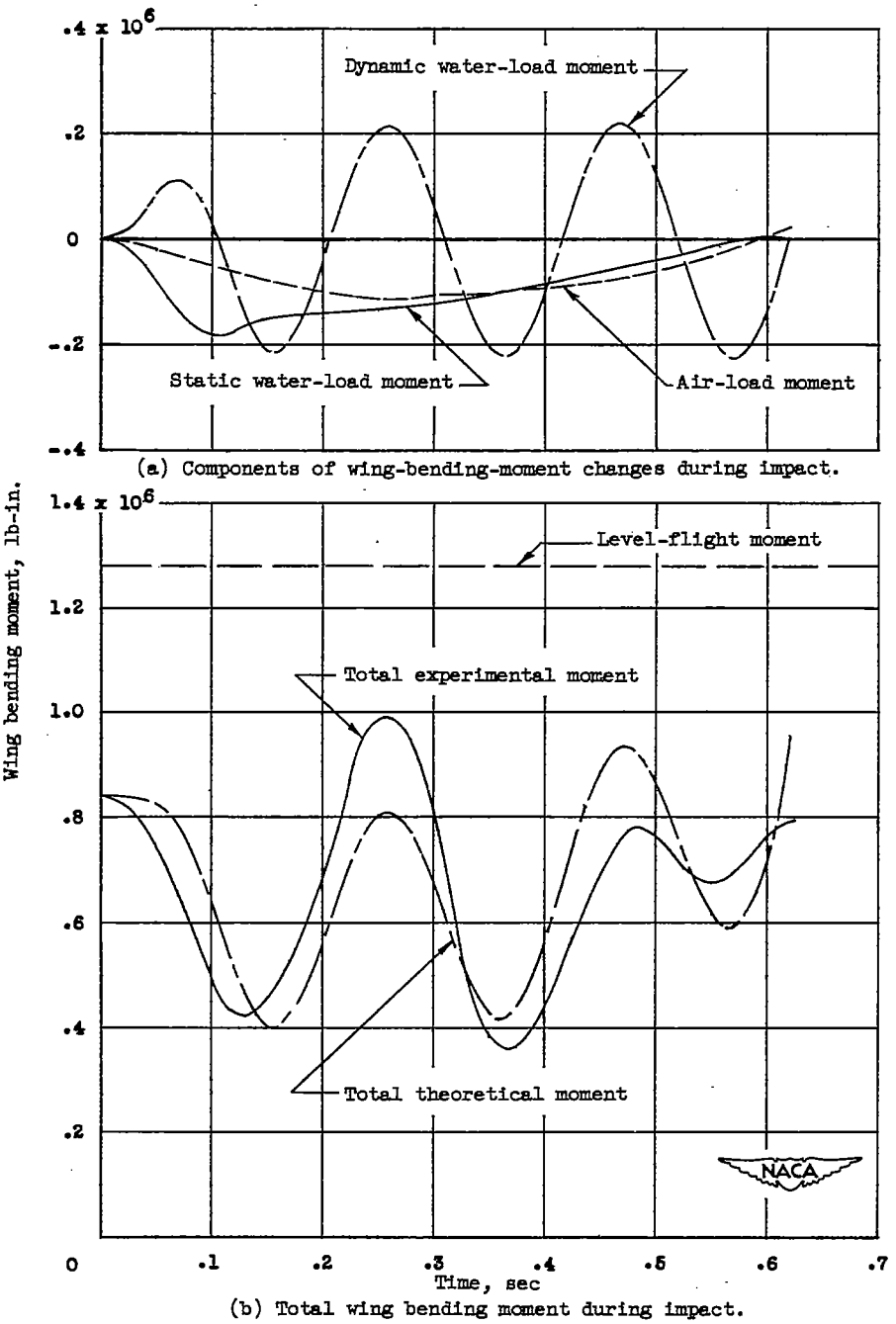

(a) Components of wing-bending-moment changes during impact.

(b) Total wing bending moment during impact.

Figure 8.- Wing-bending-moment time histories during impact, run 4.

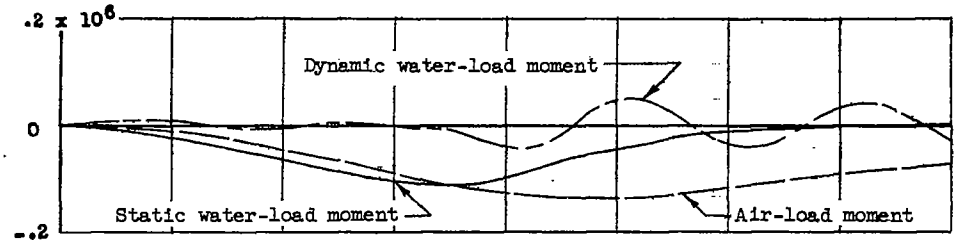

(a) Components of wing-bending-moment changes during impact.

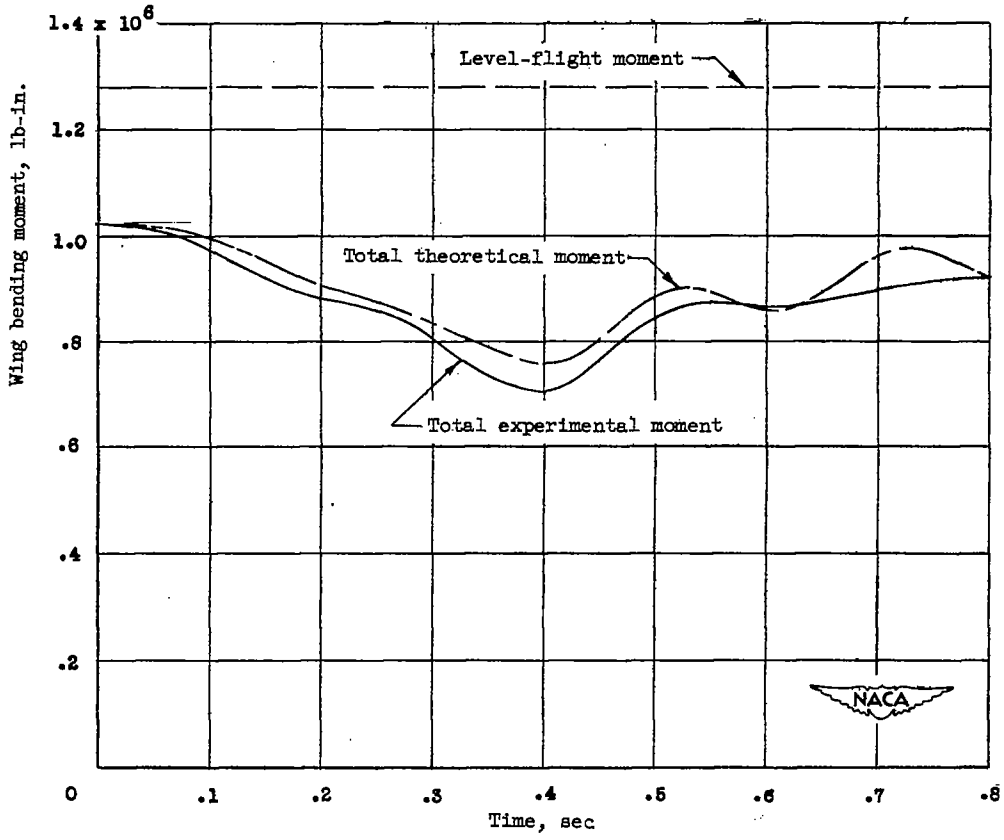

(b) Total wing bending moment during impact.

Figure 9.- Wing-bending-moment time histories during impact, run 5.

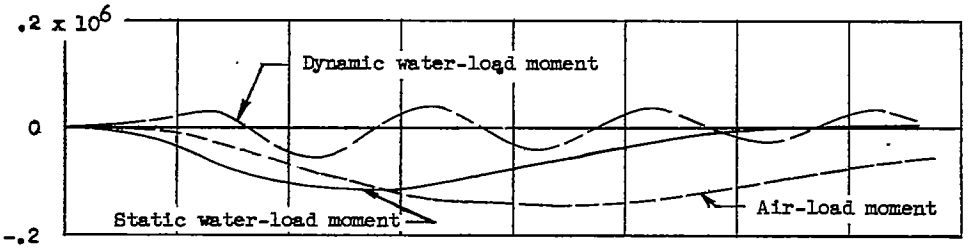

(a) Components of wing-bending-moment changes during impact.

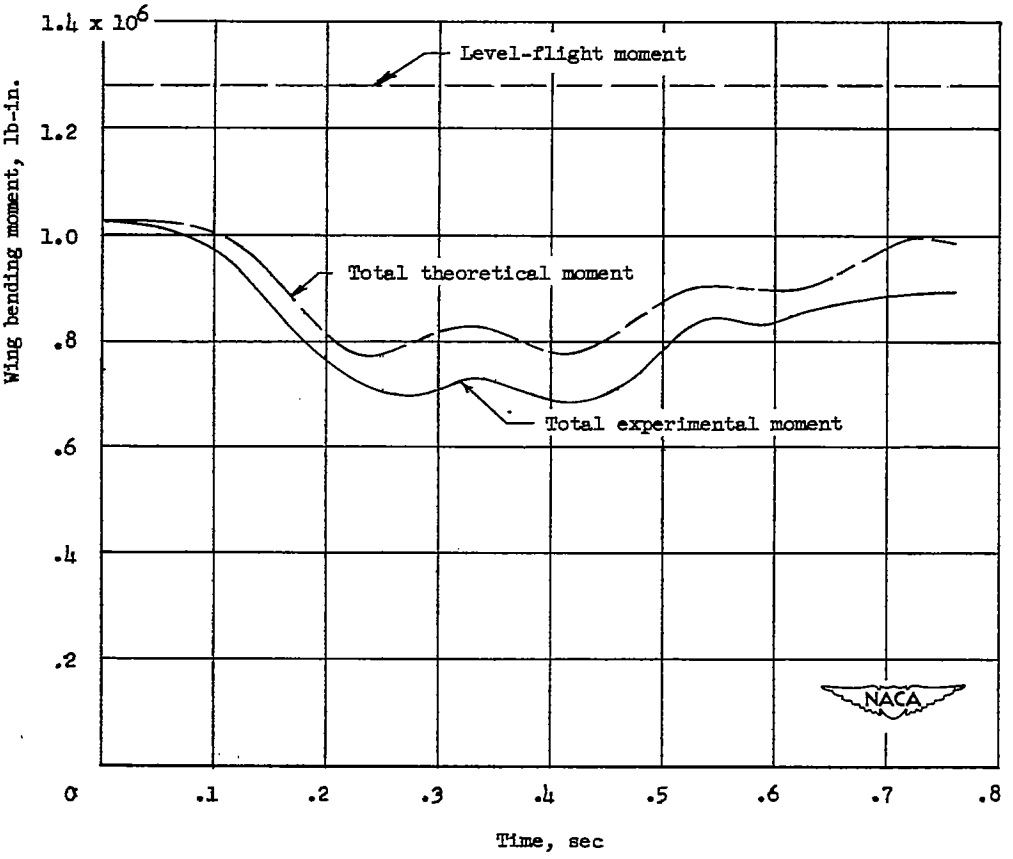

(b) Total wing bending moment during impact.

Figure 10.- Wing-bending-moment time histories during impact, run 6.

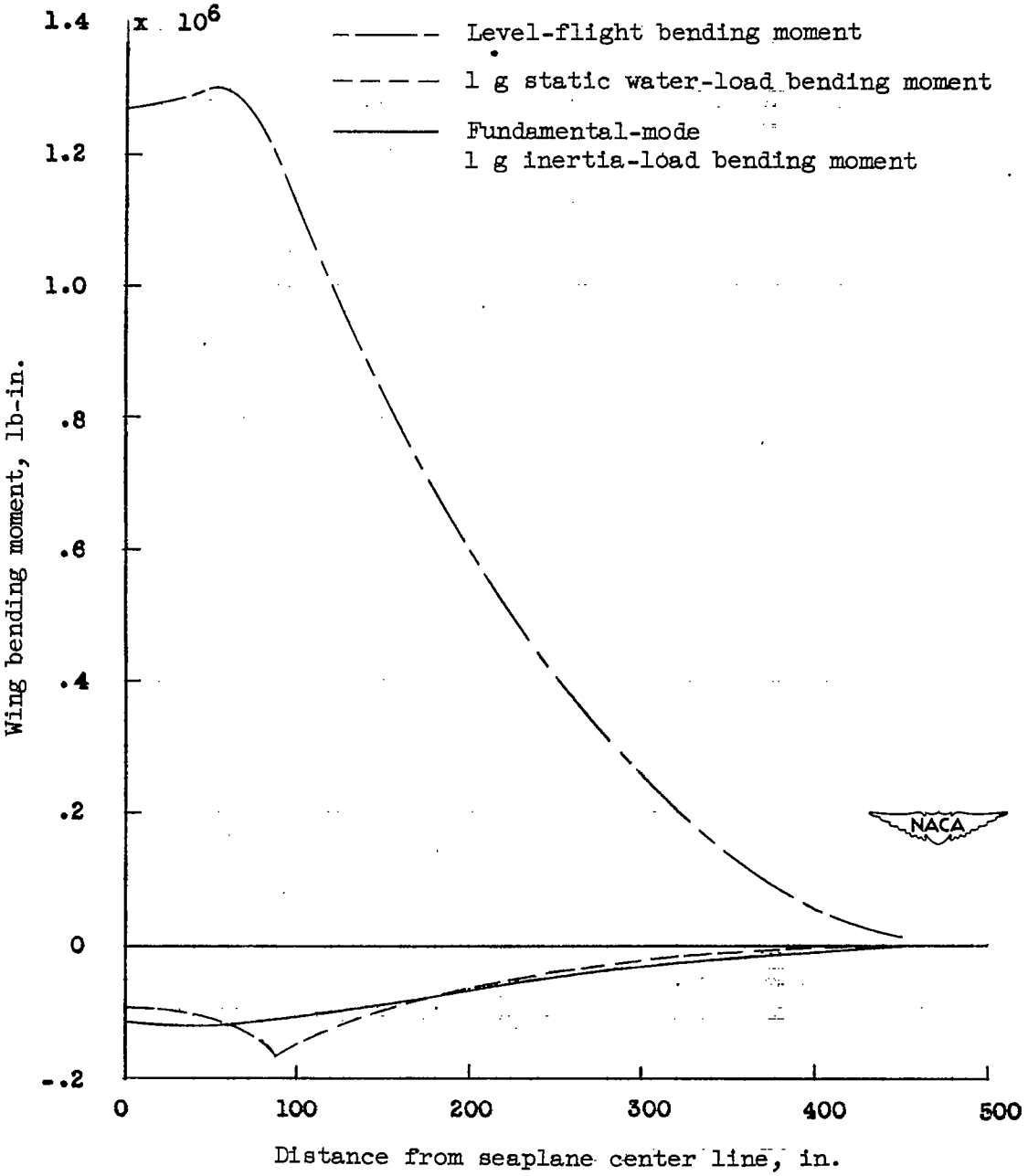

Figure 11.- Level-flight and landing-impact bending moments.

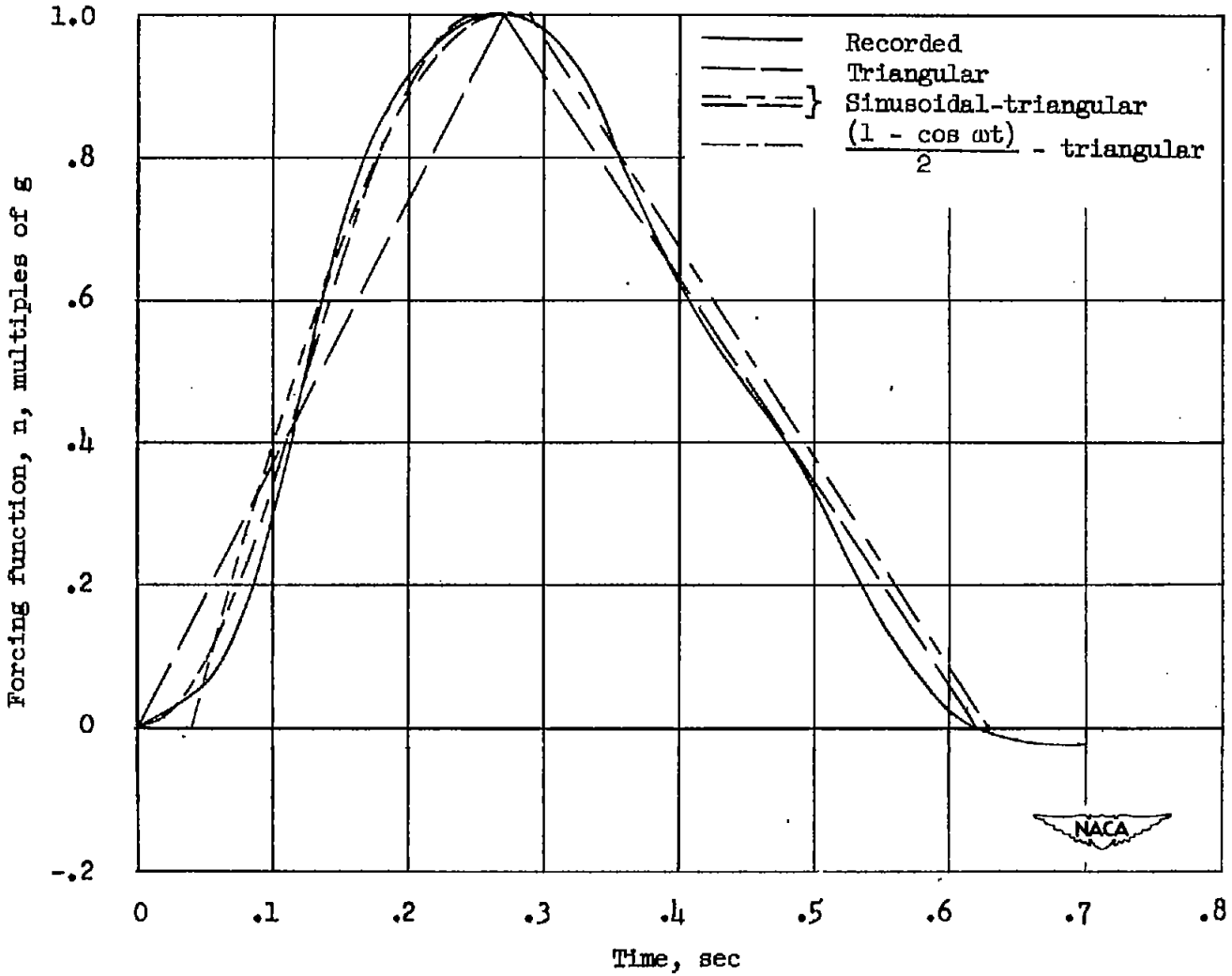

(a) Recorded forcing function and approximations.

Figure 12.- Recorded forcing function for run 4, approximations, and calculated responses.

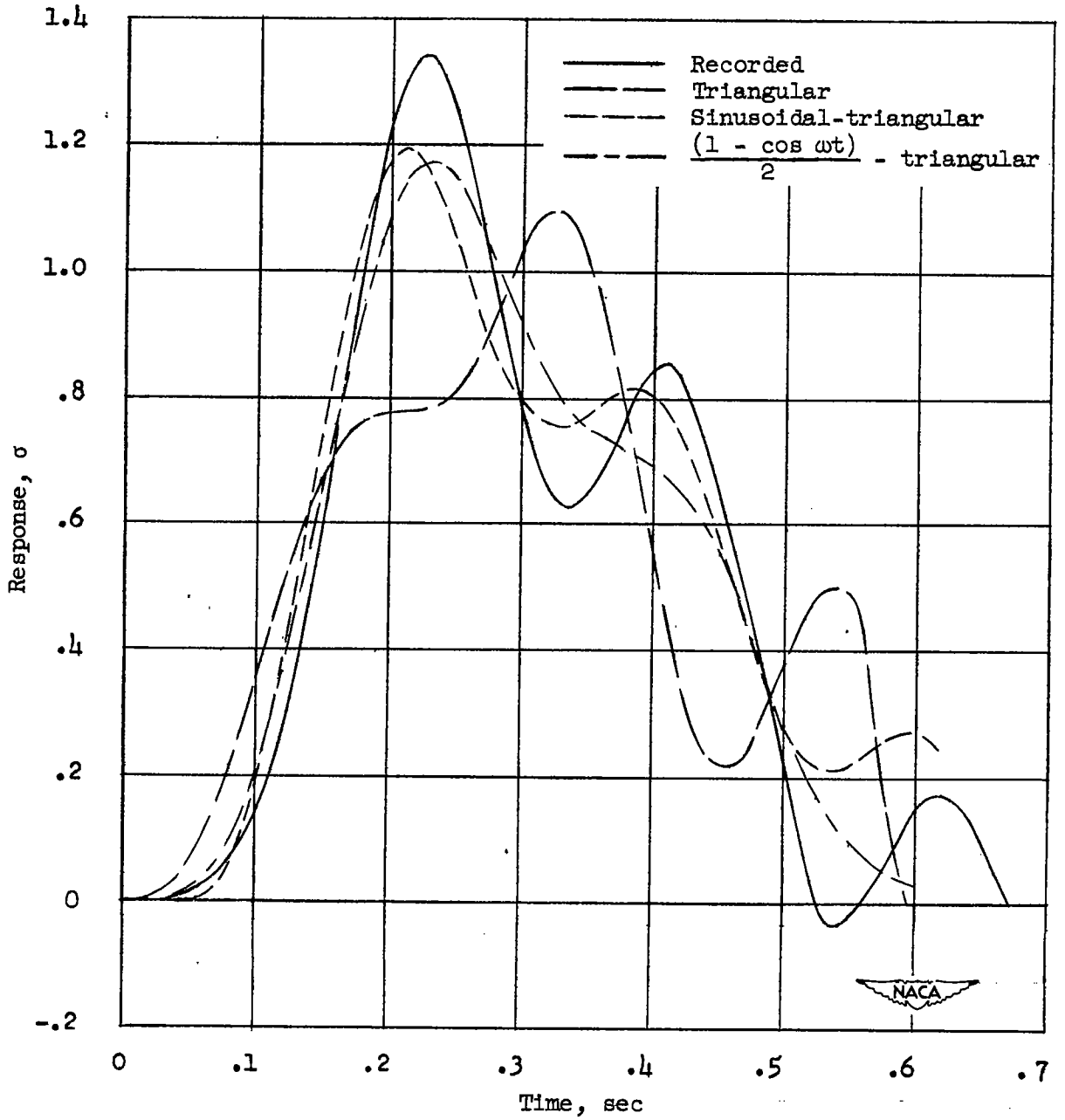

(b) Calculated responses to forcing function and approximations.

Figure 12.- Concluded.

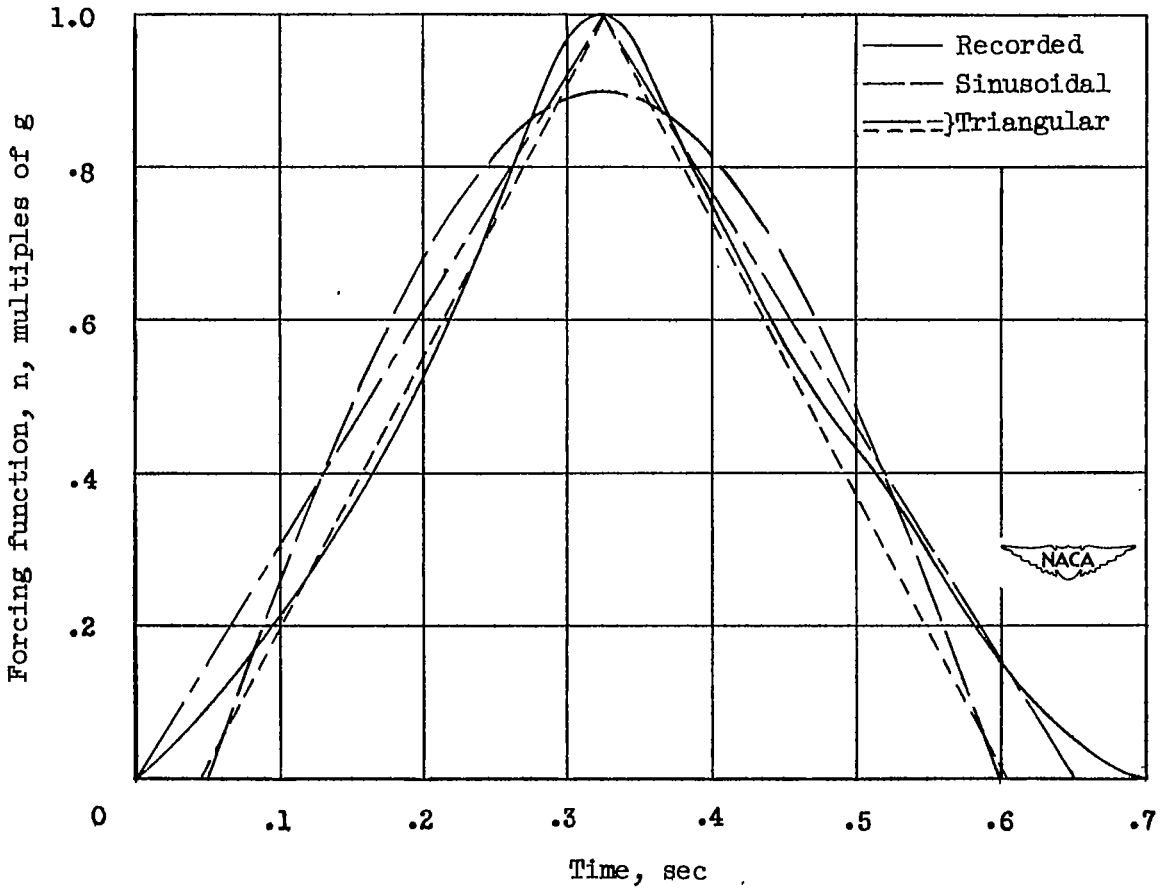

(a) Recorded forcing function and approximations.

Figure 13.- Recorded forcing function for run 5, approximations, and calculated responses.

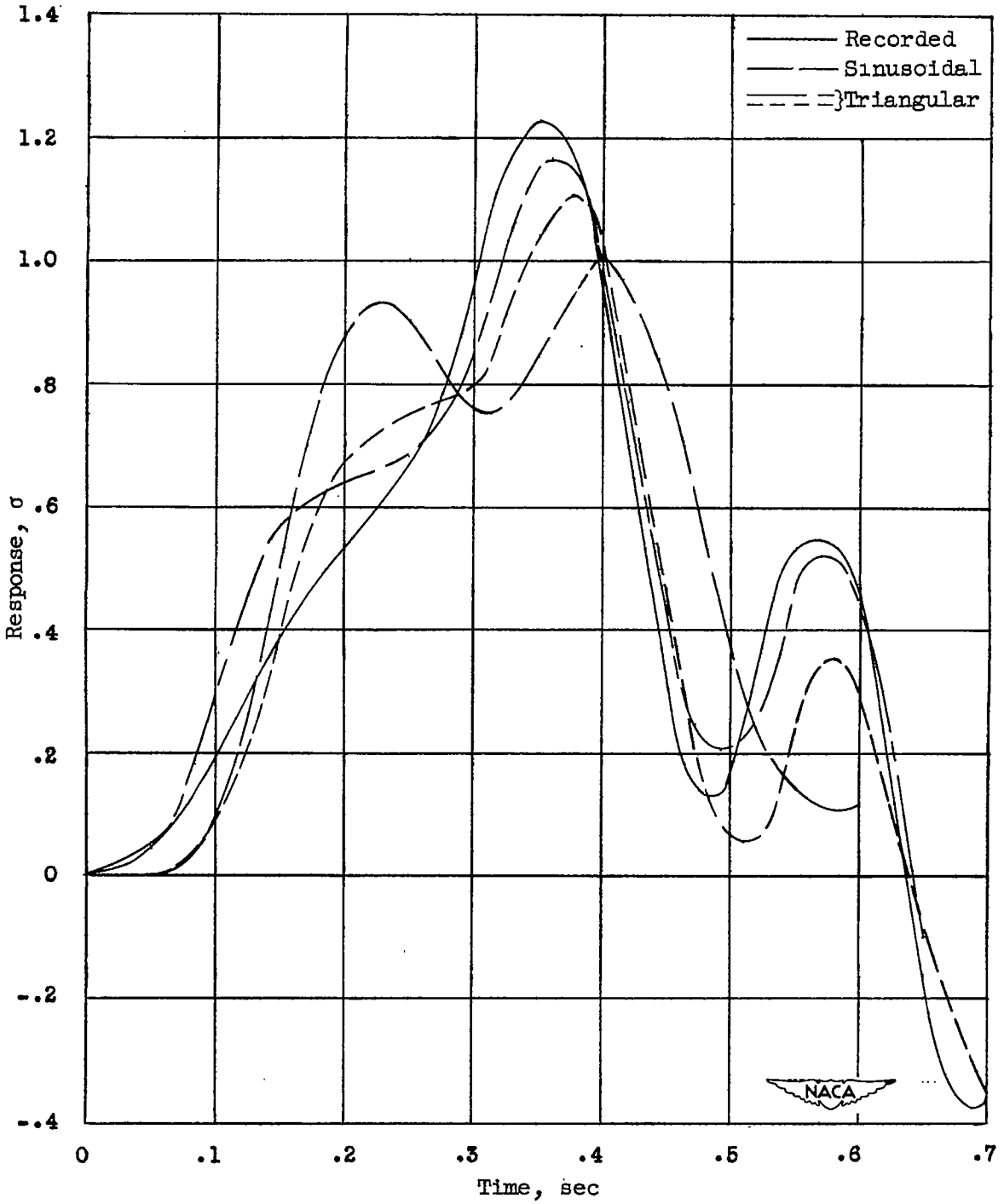

(b) Calculated responses to forcing function and approximations.

Figure 13.- Concluded.

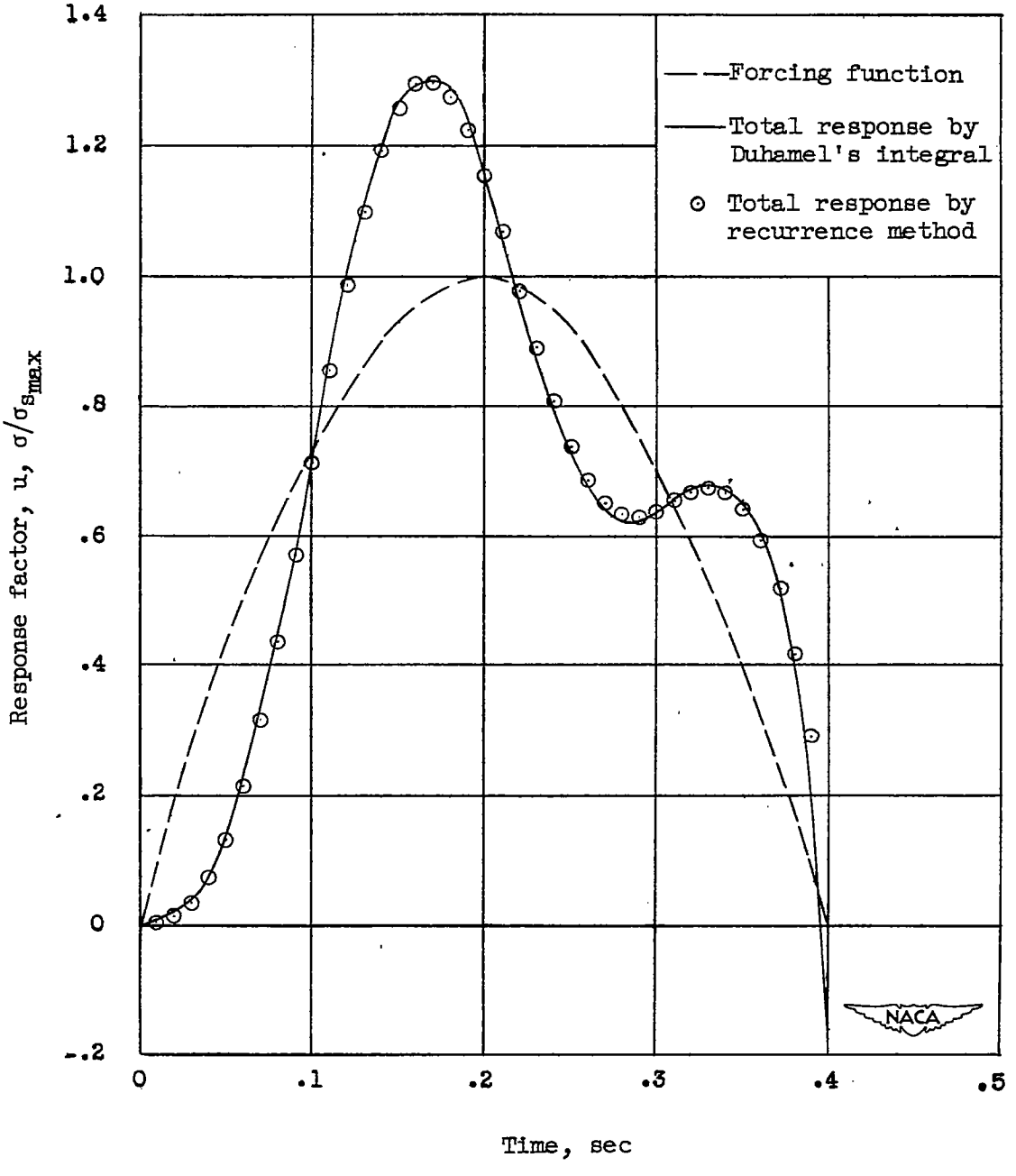

(a) Responses to sinusoidal forcing function.

Figure 14.- Comparison of total responses.

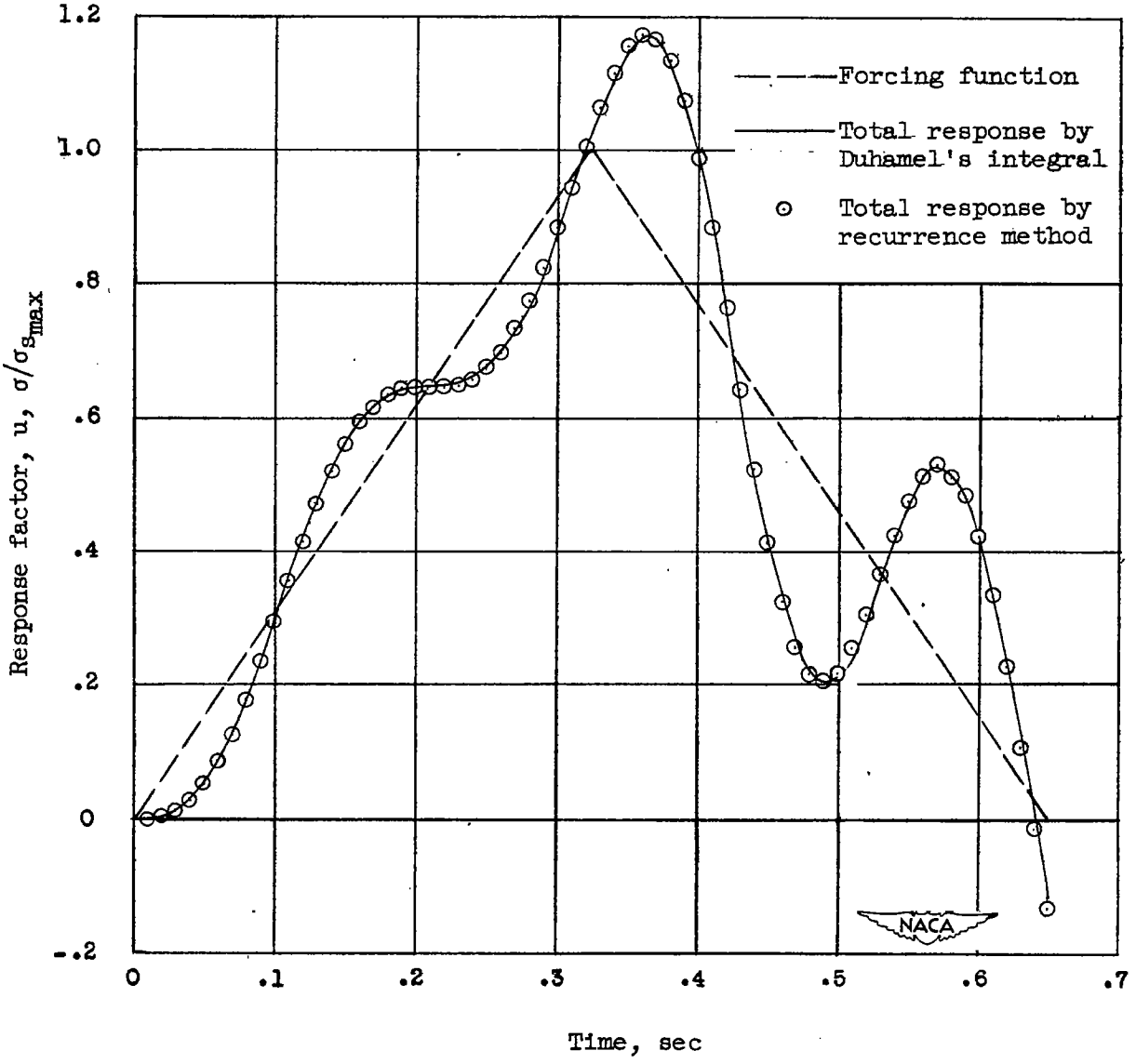

(b) Responses to triangular forcing function.

Figure 14.- Concluded.